Acta Mech 225, 2345–2362 (2014)
DOI 10.1007/s00707-014-1120-6

Xia Li · Hai-Sui Yu

Fabric, force and strength anisotropies in granular materials: a micromechanical insight

Received: 31 January 2013 / Revised: 2 December 2013 / Published online: 29 April 2014

Abstract In micromechanics, the stress–force–fabric (SFF) relationship is referred to as an analytical expression linking the stress state of a granular material with microparameters on contact forces and material fabric. This paper employs the SFF relationship and discrete element modelling to investigate the micromechanics of fabric, force and strength anisotropies in two-dimensional granular materials. The development of the SFF relationship is briefly summarized while more attention is placed on the strength anisotropy and deformation non-coaxiality. Due to the presence of initial anisotropy, a granular material demonstrates a different behaviour when the loading direction relative to the direction of the material fabric varies. Specimens may go through various paths to reach the same critical state at which the fabric and force anisotropies are coaxial with the loading direction. The critical state of anisotropic granular material has been found to be independent of the initial fabric. The fabric anisotropy and the force anisotropy approach their critical magnitudes at the critical state. The particle-scale data obtained from discrete element simulations of anisotropic materials show that in monotonic loading, the principal force direction quickly becomes coaxial with the loading direction (i.e. the strain increment direction as applied). However, material fabric directions differ from the loading direction and they only tend to be coaxial at a very large shear strain. The degree of force anisotropy is in general larger than that of fabric anisotropy. In comparison with the limited variation in the degree of force anisotropy with varying loading directions, the fabric anisotropy adapts in a much slower pace and demonstrates wider disparity in the evolution in the magnitude of fabric anisotropy. The difference in the fabric anisotropy evolution has a more significant contribution to strength anisotropy than that of force anisotropy. There are two key parameters that control the degree of deformation non-coaxiality in granular materials subjected to monotonic shearing: the ratio between the degrees of fabric anisotropy and that of force anisotropy and the angle between the principal fabric direction and the applied loading direction.

Presented at the 8th European Solid Mechanics Conference in the Graz University of Technology, Austria, 9–13 July 2012.

X. Li (✉)
Fluids and Particle Processes Group, Manufacturing and Process Technologies Research Division,
Faculty of Engineering, The University of Nottingham, University Park, Nottingham, NG7 2RD, UK
E-mail: xia.li@nottingham.ac.uk
Tel.: +44-115-9514167
Fax: +44-115-9513898
URL: www.nottingham.ac.uk/∼evzxl

H.-S. Yu
Nottingham Centre for Geomechanics, Materials, Mechanics and Structures Research Division,
Faculty of Engineering, The University of Nottingham, University Park, Nottingham, NG7 2RD, UK
E-mail: hai-sui.yu@nottingham.ac.uk
Tel.: +44-115-8466884
Fax: +44-115-9513898
URL: http://www.nottingham.ac.uk/engineering/departments/civeng/people/hai-sui.yu

1 Introduction

Granular materials have anisotropic structures either formed during natural geological processes or resulting from various in situ loading conditions. Extensive experimental and in situ data have shown the significant effect of material anisotropy on the observed stress–strain responses. For example, a cross-anisotropic sand sample, which can sustain a high shear stress when loaded vertically, may yield and even collapse when the same loading is applied horizontally [21,46]. Strength anisotropy is of key engineering importance in estimating the stability of infrastructures and has therefore attracted much research interest. Extensive efforts of experimental testing and constitutive modelling have been made to better estimate the strength and deformation of anisotropic granular soils [2,3,5,6,9,19,22,27,29,32,34,42]. Experiments have been carried out by preparing and testing specimens of different tilting angles or loading a soil specimen along various directions [20,29,30,45]. In addition, numerical simulations using discrete element methods [8] are reported and found in qualitative agreement with laboratory observations [22,31,41].

Another interesting phenomenon associated with anisotropic soil behaviour is deformation non-coaxiality, which is defined as the non-coincidence between the principal stress directions and the principal strain increment directions [1,11,36,44,47]. It was firstly observed in Roscoe et al. [36] and later widely reported for soil tests involving rotation of stress directions [13], for example, using a hollow cylindrical apparatus. The angle between the principal stress direction and the principal direction of plastic strain rate is referred to as the degree of non-coaxiality.

Material anisotropy is believed to be the main reason causing strength anisotropy and deformation non-coaxiality. However, this issue may not be fully addressed in continuum mechanics by only considering a granulate soil as an equivalent continuum. Multi-scale approaches treating a granular material as an assembly of discrete particles have been developed over the past few decades. It has become increasingly popular as particle-scale information has been made more accessible nowadays [10,14,18]. The fabric tensor has been proposed to characterize material structure and incorporated in constitutive model development to better capture the material behaviour [27,33,40,42]. Challenges remain on establishing the correlation between the proposed fabric tensors and the key characteristics of material constitutive behaviours.

Rothenburg and Selvadurai [39] were among the first to introduce Fourier series in the description of the directional variation of contact normal density. They further derived the stress–force–fabric (SFF) relationship for two-dimensional assemblies consisting of discs [37], and later extended the expression to two-dimensional elliptical-shaped particles [38] and three-dimensional ellipsoidal particles with anisotropy tensors [35]. The SFF relationship proposed by Rothenberg and his co-workers expressed the macroscopic stress tensor with an explicit statistical description in terms of microscopic parameters. It is an analytical relationship providing micromechanical insight into the stress state of granular materials.

Recently, Li and Yu [24] employed the theory of directional statistics to study the statistics of particle-scale information. They revisited the assumptions made in Rothenburg and his co-workers' derivation and proposed a more general form of the SFF relationship using tensor multiplication. The form of polynomial expansions in direction $\mathbf{n}$ proposed in Kanatani [16,17] was followed to approximate the directional distributions of contact normal density, mean contact vector and mean contact force. The least square error criterion was employed to determine the tensorial coefficients, i.e. the direction tensors. These direction tensors are macroscopic variables representing the particle-scale statistics. The SFF relationship and the theory of directional statistics are useful tools in studying the micromechanics and exploring the micro–macro relationships of granular materials. Following a brief summary of this new development, this paper applies them to study the micromechanics of anisotropic granular materials.

In a study of the dependence of granular material behaviour on initial fabric and loading directions, Li and Yu [22] prepared and tested two anisotropic specimens consisting of non-spherical particles using a two-dimensional commercial discrete element package, Particle Flow Code in Two Dimensions (PFC2D) [15]. Observations were made on strength anisotropy and deformation non-coaxiality for both specimens. Multi-scale data obtained from Li and Yu [22] will be used here, where appropriate, to facilitate our discussion in this paper.

2 A summary of the SFF relationship

In this paper, an Einstein summation convention is adopted for repeated subscripts unless indicated otherwise.

2.1 The derivation of the SFF relationship

Treating a granular material as an assembly of granular particles with only point contact interactions and volume forces, the macro-stress tensor can be evaluated from the tensor product of contact forces f_i^c and contact vectors v_i^c as follows:

$$\sigma_{ij} = \frac{1}{V} \sum_{c \in V} v_i^c f_j^c, \tag{1}$$

in which σ_{ij} stands for the average stress over volume V [4,7,12,26,28,39,43]. To be consistent with the sign convention in soil mechanics, a contact vector is defined here as the vector pointing from the contact point to the particle centre. Equation (1) was established based on Newton's second law of motion and is subject to no constraints on particle or sample geometries. For each internal contact point between the particles P and Q, there is always a pair of action and reaction forces in association with two contact vectors pointing from the contact point to each of the particle centres. They are accounted as two contacts and contribute to Eq. (1) as two separate terms.

In granular mechanics, contact direction is important. Denoting the contact normal direction as $\mathbf{n}$, a unit direction vector normal to the particle surface at the contact point, the terms on the right-hand side of Eq. (1) can be grouped according to their contact normal directions, leading to

$$\sigma_{ij} = \frac{1}{V} \sum_{\Omega} \langle v_i f_j \rangle |_{\mathbf{n}} \Delta M(\mathbf{n}) = \frac{M}{V} \sum_{\Omega} e^c(\mathbf{n}) \langle v_i f_j \rangle |_{\mathbf{n}} \Delta\Omega, \tag{2}$$

where Ω represents the unit circle in two-dimensional spaces ($D = 2$) and the unit sphere in three-dimensional spaces ($D = 3$). $*|_{\mathbf{n}}$ denotes the value of variable $*$ in direction $\mathbf{n}$, and $\langle * \rangle |_{\mathbf{n}}$ denotes the average value of all terms of $*$ sharing the same contact normal direction $\mathbf{n}$. The total number of contacts is denoted as M, and $\Delta M(\mathbf{n})$ represents the number of contacts whose normal directions fall into the stereo-angle element $\Delta\Omega$ centred at direction $\mathbf{n}$. $e^c(\mathbf{n}) = \Delta M(\mathbf{n})/\Delta\Omega$ is the probability density function of contact normals. The average number of contacts per particle is $\omega = M/N$, where N is the total number of particles. In the case of thermodynamic limit, ω approaches a limit, i.e. $\lim_{N\to\infty} M/N = \omega$. It is referred to as the coordination number, an index characterizing the packing density.

When $\Delta\Omega \to 0$, the transition leads to an expression of the stress tensor in terms of integration over all stereo-angles as follows:

$$\sigma_{ij} = \frac{\omega N}{V} \oint_{\Omega} e^c(\mathbf{n}) \langle v_i f_j \rangle |_{\mathbf{n}} \mathrm{d}\Omega, \tag{3}$$

where $\mathrm{d}\Omega$ is an elementary solid angle. Equation (3) is a directional integration over the product of the contact normal probability density $e^c(\mathbf{n})$ and the joint product $\langle v_i f_j \rangle |_{\mathbf{n}}$.

Equation (3) involves the joint product $\langle v_i f_j \rangle |_{\mathbf{n}}$ within the integration. In general, $\langle v_i f_j \rangle |_{\mathbf{n}} \neq \langle v_i \rangle |_{\mathbf{n}} \langle f_j \rangle |_{\mathbf{n}}$, where $\langle v_i \rangle |_{\mathbf{n}}$ and $\langle f_j \rangle |_{\mathbf{n}}$ denote the mean contact vector and the mean contact force along direction $\mathbf{n}$, respectively. The statistical dependence between them can be investigated by comparing the directional distribution of $\langle v_i f_j \rangle |_{\mathbf{n}}$, $\langle v_i \rangle |_{\mathbf{n}} \langle f_j \rangle |_{\mathbf{n}}$ [24]. The observation supports the assumption that the statistical dependence between contact vectors and contact forces can be considered isotropic. This is the first simplification made in the derivation of the SFF relationship.

Simplification 1 The effect of the statistical dependence between contact vectors and contact forces could be taken into account by approximating:

$$\langle v_i f_j \rangle |_{\mathbf{n}} = \varsigma \langle v_i \rangle |_{\mathbf{n}} \langle f_j \rangle |_{\mathbf{n}} \tag{4}$$

with ς a direction independent scalar.

Applying the directional statistic theory [16,23], directional distributions, such as $e^c(\mathbf{n})$, $\langle v_i \rangle |_{\mathbf{n}}$ and $\langle f_i \rangle |_{\mathbf{n}}$, can be approximated in terms of polynomials of unit directional vector $\mathbf{n}$. Normally, only a limited number of terms is necessary for approximation. Statistical analyses were carried out to process the microscale data obtained in 2D DEM simulations reported in [22]. The results suggested that it is sufficient to approximate the directional distributions of contact normal density, mean contact forces and mean contact vectors with up to 2nd, 3rd and 1st ranks of power terms of direction vector $\mathbf{n}$ [24]. This supports the following three simplifications.

Simplification 2 The contact normal density $e^c(\mathbf{n})$ can be sufficiently approximated with up to 2nd ranks of power terms of the direction vector $\mathbf{n}$ as follows:

$$E^c(\mathbf{n}) = \frac{1}{E_0}\left(D_0 + D^c_{i_1 i_2} n_{i_1} n_{i_2}\right), \tag{5}$$

where $D^c_{i_1 i_2}$ is the 2nd rank deviatoric direction tensor for contact normal density. It is a deviatoric and symmetric tensor.

Simplification 3 The mean contact force $\langle \mathbf{f} \rangle|_{\mathbf{n}}$ can be sufficiently approximated with up to 3rd ranks of power terms of the direction vector $\mathbf{n}$ as:

$$F_j(\mathbf{n}) = f_0\left(n_j + G^f_{ji_1} n_{i_1} + G^f_{ji_1 i_2 i_3} n_{i_1} n_{i_2} n_{i_3}\right), \tag{6}$$

where $G^f_{ji_1}$ and $G^f_{ji_1 i_2 i_3}$ are the deviatoric direction tensors for the 1st rank and 3rd rank polynomial terms in the approximation. They are deviatoric tensors, and $G^f_{ji_1 i_2 i_3}$ is symmetric with respect to the subscripts i_1, i_2, i_3.

Simplification 4 The mean contact vector $\langle \mathbf{v} \rangle|_{\mathbf{n}}$ can be sufficiently approximated with up to 1st ranks of power terms of the direction vector $\mathbf{n}$ as:

$$V_j(\mathbf{n}) = v_0\left(n_j + G^v_{ji_1} n_{i_1}\right), \tag{7}$$

where $G^v_{ji_1}$ is the deviatoric direction tensors for the first rank polynomial term in the approximation. It is again a deviatoric tensor.

With the above simplifications, the directional integration in Eq. (3) can be achieved in terms of tensor multiplication, leading to:

$$\sigma_{ij} = \frac{\omega N}{V} \varsigma v_0 f_0 \left[\begin{array}{l} \alpha_2\left(\delta_{ij} + G^f_{ji} + G^v_{ij} + G^f_{jl_1} G^v_{il_1}\right) \\ \quad + \frac{2}{3}\alpha_4\left(D^c_{ij} + D^c_{im_1} G^f_{jm_1} + D^c_{im_1} G^v_{jm_1} + D^c_{l_1 m_1} G^v_{il_1} G^f_{jm_1}\right) \\ \quad + \frac{2}{5}\alpha_6\left(D^c_{k_1 k_2} G^f_{jik_1 k_2} + D^c_{k_1 k_2} G^v_{il_1} G^f_{jl_1 k_1 k_2}\right) \end{array}\right], \tag{8}$$

where $\alpha_{2n} = \begin{cases} \frac{^{2n}C_n}{2^{2n}}, D = 2 \\ \frac{1}{2n+1}, D = 3 \end{cases}$ and ^nC_k stands for the number of k-combinations of an n-element set [24]. Equation (8) is valid for both two-dimensional spaces and three-dimensional spaces for granular materials of various particle shapes, as long as the above four simplifications are considered reasonable.

2.2 Two-dimensional SFF relationship in terms of Fourier Expansions

2.2.1 Contact normal density $e^c(\mathbf{n})$

In two-dimensional conditions, the unit direction vector $\mathbf{n}$ can be represented as $\mathbf{n} = (\cos\theta, \sin\theta)$ in terms of the angle θ in the given coordinate system. For contact normal density, the deviatoric direction tensor of the second-order power term can be represented as

$$D^c_{i_1 i_2} = d^c_2 \begin{pmatrix} \cos\phi^c_2 & \sin\phi^c_2 \\ \sin\phi^c_2 & -\cos\phi^c_2 \end{pmatrix}, \tag{9}$$

where d^c_2 denotes the magnitude of directional variation, and $\phi^c_2/2$ indicates the preferred principal direction, as exemplified in Fig. 1. Simplification 2 implies that the directional distributions of contact normal density could be approximated as

$$E^c(\mathbf{n}) = \frac{1}{2\pi}\left[1 + d^c_2 \cos\left(2\theta - \phi^c_2\right)\right]. \tag{10}$$

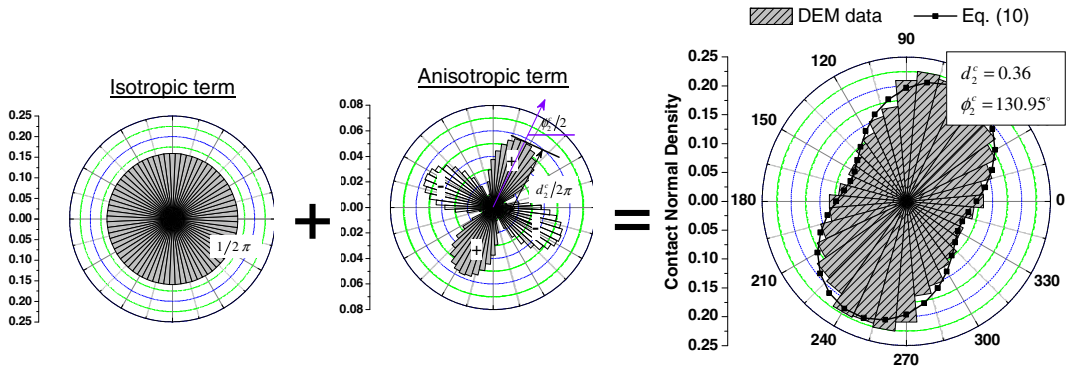

Fig. 1 Directional distribution of contact normal density $e^c(\mathbf{n})$

It is the summation of an isotropic component and an anisotropic component as shown in Fig. 1.

Now we will make use of the particle-scale information obtained from Li and Yu [22] for illustration. The approximation using Eq. (10) is plotted in Fig. 1 together with the data directly obtained from DEM simulation. When the initially anisotropically specimen was sheared at $\alpha = 45°$ up to 2 % of deviatoric strain, it is calculated that $d_2^c = 0.36$, $\phi_2^c = 131°$, as indicated in the figure.

2.2.2 *Mean contact force* $\langle \mathbf{f} \rangle |_{\mathbf{n}}$

For mean contact forces, Li and Yu [24] showed that Eq. (6) is sufficient and the two-dimensional deviatoric direction tensors for the 1st rank and 3rd rank terms in the approximation take the form

$$G^f_{ji_1} = B^f_1 \begin{pmatrix} \cos\beta^f_1 & \sin\beta^f_1 \\ \sin\beta^f_1 & -\cos\beta^f_1 \end{pmatrix}, \quad G^f_{ji_111} = A^f_3 \begin{pmatrix} \cos\alpha^f_3 & \sin\alpha^f_3 \\ -\sin\alpha^f_3 & \cos\alpha^f_3 \end{pmatrix}, \tag{11}$$

where B^f_1 and A^f_3 denote the magnitudes of directional variation, β^f_1 and α^f_3 give information on the preferable directions.

Simplification 3 suggests that the mean contact force could be approximated as

$$\langle \mathbf{f} \rangle |_{\mathbf{n}} = f_0 \left[\begin{pmatrix} \cos\theta \\ \sin\theta \end{pmatrix} + B^f_1 \begin{pmatrix} \cos\left(\theta - \beta^f_1\right) \\ -\sin\left(\theta - \beta^f_1\right) \end{pmatrix} + A^f_3 \begin{pmatrix} \cos\left(3\theta - \alpha^f_3\right) \\ \sin\left(3\theta - \alpha^f_3\right) \end{pmatrix} \right]. \tag{12}$$

Decomposing the mean contact force into a normal component and a tangential component, we have

$$\langle f^n \rangle |_\theta = f_0 \left[1 + B^f_1 \cos\left(2\theta - \beta^f_1\right) + A^f_3 \cos\left(2\theta - \alpha^f_3\right) \right] = f_0 \left[1 + C^f_n \cos\left(2\theta - \phi^f_n\right) \right], \tag{13}$$

$$\langle f^t \rangle |_\theta = f_0 \left[-B^f_1 \sin\left(2\theta - \beta^f_1\right) + A^f_3 \sin\left(2\theta - \alpha^f_3\right) \right] = -f_0 C^f_t \sin\left(2\theta - \phi^f_t\right), \tag{14}$$

where $C^f_n = \sqrt{B^{f2}_1 + A^{f2}_3 + 2B^f_1 A^f_3 \cos\left(\beta^f_1 - \alpha^f_3\right)}$, $\tan\phi^f_n = \left(B^f_1 \sin\beta^f_1 + A^f_3 \sin\alpha^f_3\right) \Big/ \left(B^f_1 \cos\beta^f_1 + A^f_3 \cos\alpha^f_3\right)$, $C^f_t = \sqrt{B^{f2}_1 + A^{f2}_3 - 2B^f_1 A^f_3 \cos\left(\beta^f_1 - \alpha^f_3\right)}$ and $\tan\phi^f_t = \left(B^f_1 \sin\beta^f_1 - A^f_3 \sin\alpha^f_3\right) \Big/ \left(B^f_1 \cos\beta^f_1 - A^f_3 \cos\alpha^f_3\right)$. The mean normal contact force and the mean tangential contact force are sinusoidal functions with period π, while the magnitudes and phase angles for normal and tangential forces may not necessarily be the same. The parameters in Eqs. (13) and (14) are indicated in Fig. 2 to exemplify directional distributions of normal and tangential contact forces.

When the initially anisotropic specimen is sheared up to 2 % of deviatoric strain, the deviatoric direction tensor for contact forces is calculated with $f_0 = 0.078N$, $B^f_1 = 0.35$, $\beta^f_1 = 98°$, $A^f_3 = 0.09$, $\alpha^f_3 = 106°$ and $c^f_n = 0.44$, $\phi^f_n = 100°$, $c^f_t = 0.26$, $\phi^f_t = 96°$. Substituting these parameters into Eqs. (13) and (14) gives the approximation of mean contact forces. They are plotted in Fig. 2 together with actual DEM data for comparison.

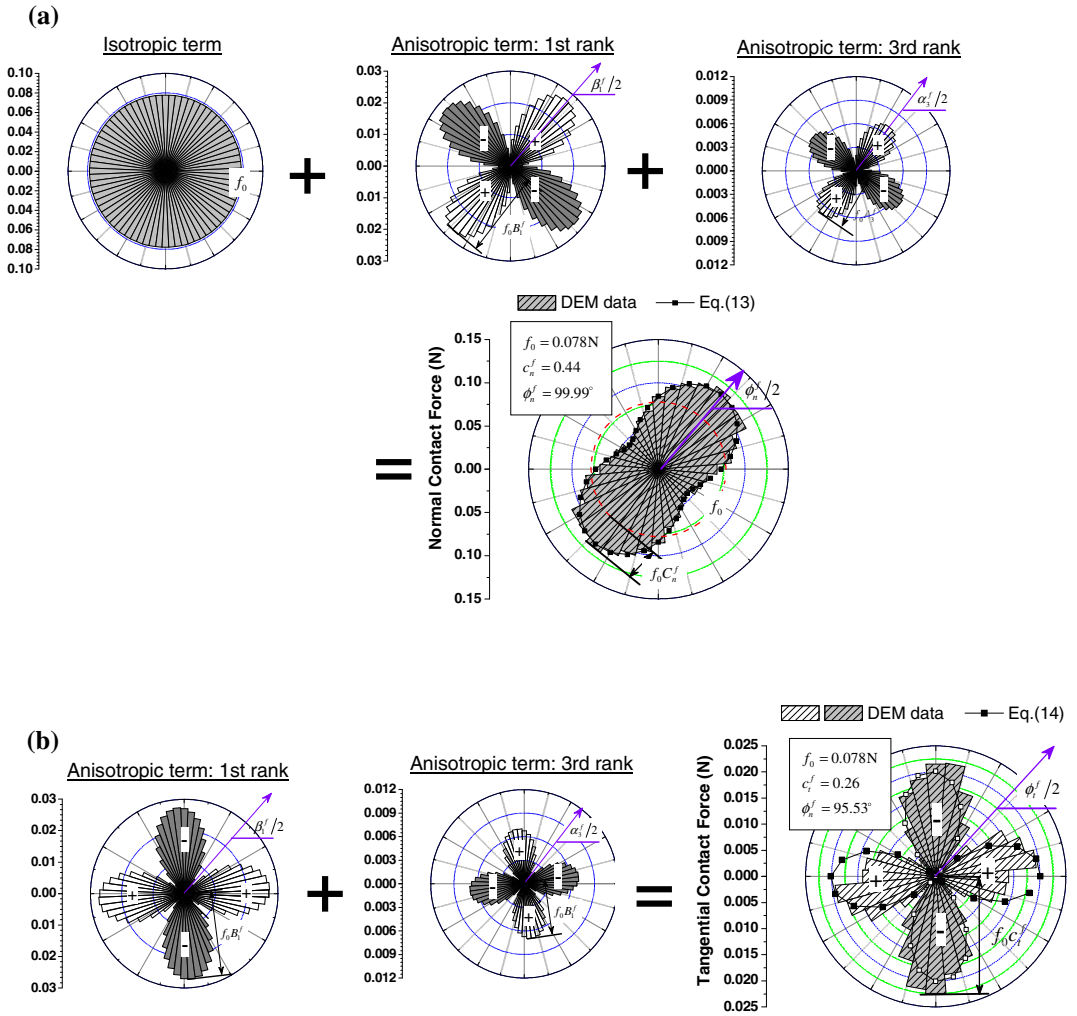

Fig. 2 Approximation of mean contact force $\langle \mathbf{f} \rangle|_{\mathbf{n}}$ with Eqs. (13) and (14). **a** Mean normal contact force. **b** Mean tangential contact force

2.2.3 Mean contact vector $\langle \mathbf{v} \rangle|_{\mathbf{n}}$

The two-dimensional deviatoric direction tensors for the 1st rank term in the approximation of mean contact vectors can be expressed as

$$G^v_{ji_1} = B^v_1 \begin{pmatrix} \cos\beta^v_1 & \sin\beta^v_1 \\ \sin\beta^v_1 & -\cos\beta^v_1 \end{pmatrix}, \tag{15}$$

where B^v_1 denotes the magnitude of directional variation, β^v_1 indicates the preferable direction. The magnitudes and the phase angles for the normal and tangential components are equal because only the 1st rank term is used here for approximation.

Simplification 4 suggests that the directional distributions of mean contact vectors can be sufficiently approximated as

$$\langle \mathbf{v} \rangle|_\theta = v_0 \left[\begin{pmatrix} \cos\theta \\ \sin\theta \end{pmatrix} + B^v_1 \begin{pmatrix} \cos\left(\theta - \beta^v_1\right) \\ -\sin\left(\theta - \beta^v_1\right) \end{pmatrix} \right]. \tag{16}$$

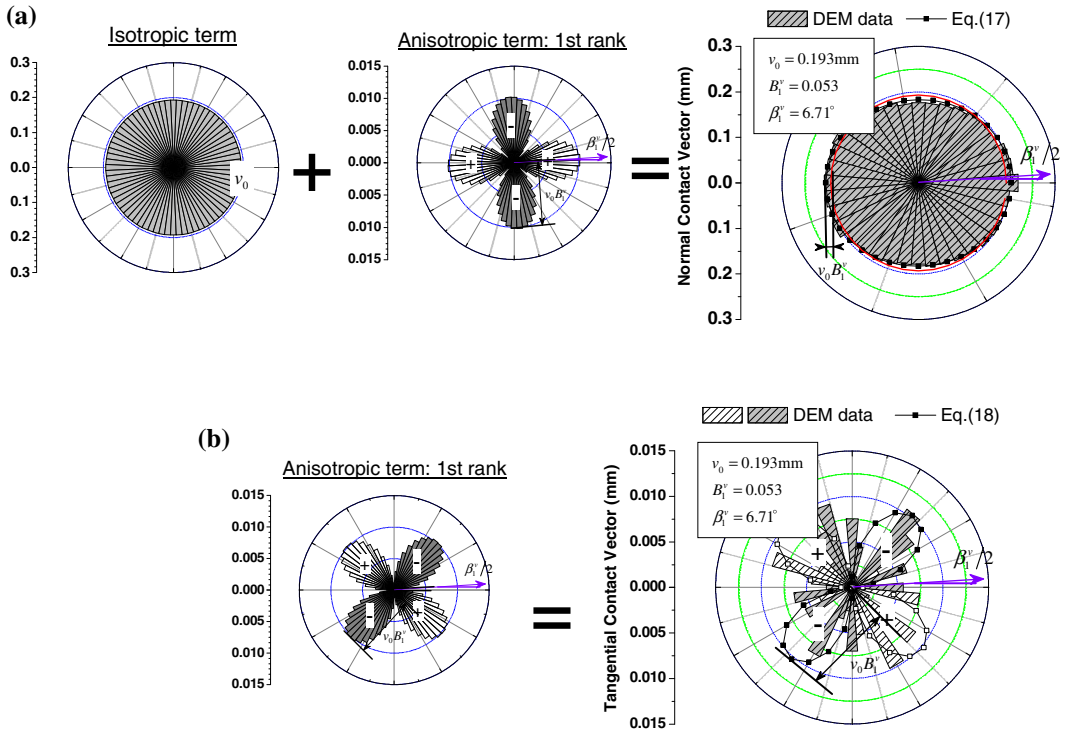

Fig. 3 Approximation of mean contact vector $\langle \mathbf{v} \rangle |_{\mathbf{n}}$ with Eqs. (17) and (18). **a** Mean normal contact vector. **b** Mean tangential contact vector

Decomposing the mean contact vector $\langle \mathbf{v} \rangle |_{\mathbf{n}}$ into a normal component and a tangential component leads to:

$$\langle v^n \rangle |_\theta = v_0 \left[1 + B_1^v \cos\left(2\theta - \beta_1^v \right) \right], \tag{17}$$

$$\langle v^t \rangle |_\theta = v_0 \left[-B_1^v \sin\left(2\theta - \beta_1^v \right) \right]. \tag{18}$$

When the initially anisotropic specimen is sheared up to 2 % of deviatoric strain, it has been calculated that $v_0 = 0.193\,\text{mm}$, $B_1^v = 0.053$, $\beta_1^f = 6.71°$. The approximations are plotted in Fig. 3 together with the information collected from DEM simulation for comparison. The disparity in the mean tangential contact vector is negligible due to the fact that the anisotropic magnitude is extremely low.

2.2.4 Simplified SFF in two dimensions

The stress tensor expression can be further simplified by invoking the symmetry in the Cauchy stress tensor, i.e. $\sigma_{12} = \sigma_{21}$. Note that the contact normal density, mean normal contact force and mean contact vector in all directions are nonnegative, and the magnitudes of the direction tensors are of limited range (between 0 and 1). Under most conditions, the triple products of the high rank terms of the three direction tensor are insignificant and can be ignored. Noticing that $D^c_{i_1 i_2}$, $G^v_{j i_1}$ and $G^f_{j i_1}$ are symmetric and deviatoric tensors, Li and Yu [24] proposed a simplified form of the SFF relationship in two-dimensional spaces:

$$\sigma_{ij} = \frac{\omega N}{2V} \varsigma v_0 f_0 \left[(1 + h)\, \delta_{ij} + G^f_{ji} + G^v_{ij} + \frac{1}{2} D^c_{ij} \right], \tag{19}$$

where $h = \frac{1}{2} G^f_{i l_1} G^v_{i l_1} + \frac{1}{4} \left(D^c_{i k_1} G^f_{i k_1} + D^c_{i k_1} G^v_{i k_1} \right) + \frac{1}{8} D^c_{k_1 k_2} G^f_{i i k_1 k_2}$ is a scalar accounting for the contribution from the joint products. It is interesting to note that $G^f_{j i_1 i_2 i_3}$ does not appear directly in Eq. (19), but contributes only to the coefficient h through the joint product $D^c_{k_1 k_2} G^f_{i i k_1 k_2}$.

With the expressions of deviatoric direction tensors given in Eqs. (9), (11) and (15), the SFF relationship in two dimensions can be expressed, in a component form, as follows:

$$\begin{cases} \sigma_{11} = \frac{\omega N}{2V}\varsigma v_0 f_0 \left[(1+h) + \left(B_1^f \cos\beta_1^f + B_1^v \cos\beta_1^v + \frac{1}{2}d_2^c \cos\phi_2^c\right)\right], \\ \sigma_{12} = \sigma_{21} = \frac{\omega N}{2V}\varsigma v_0 f_0 \left[B_1^f \sin\beta_1^f + B_1^v \sin\beta_1^v + \frac{1}{2}d_2^c \sin\phi_2^c\right], \\ \sigma_{22} = \frac{\omega N}{2V}\varsigma v_0 f_0 \left[(1+h) - \left(B_1^f \cos\beta_1^f + B_1^v \cos\beta_1^v + \frac{1}{2}d_2^c \cos\phi_2^c\right)\right]. \end{cases} \tag{20}$$

Hence, we have the expression of the mean normal stress as:

$$p = \frac{\omega N}{2V}\varsigma\,(1+h)\,v_0 f_0 \tag{21}$$

and the normalized deviatoric stress tensor as:

$$\eta_{ij} = \frac{\sigma_{ij}}{p} - \delta_{ij} = \frac{1}{1+h}\left(G_{ji}^f + G_{ij}^v + \frac{1}{2}D_{ij}^c\right). \tag{22}$$

It is symmetric and deviatoric and can be expressed in the form

$$\eta_{ij} = \frac{\eta}{2}\begin{pmatrix} \cos\theta_\sigma & \sin\theta_\sigma \\ \sin\theta_\sigma & -\cos\theta_\sigma \end{pmatrix}, \tag{23}$$

where η is the material stress ratio and $\theta_\sigma/2$ denotes the principal stress direction. The stress ratio $\eta = q/p$ is defined as the ratio of deviatoric stress q to mean normal stress p. In 2D spaces, the mean normal stress and the deviatoric stress are defined as $p = (\sigma_1 + \sigma_2)/2$ and $q = \sigma_1 - \sigma_2$, respectively, where σ_1 and σ_2 are the major and minor principal stresses.

3 Dependence of material stress on fabric anisotropy

3.1 A combined fabric tensor definition

The normalized deviatoric stress tensor, represented in Eq. (23) in terms of the stress ratio η and the principal stress direction θ_σ, can be determined by anisotropy magnitudes of material fabric and contact forces (particle interactions), and their principal directions as seen in Eq. (22). In this relationship, D_{ij}^c and G_{ij}^v are the two deviatoric direction tensors describing particle-scale geometries (i.e. the internal structure of granular materials). D_{ij}^c characterizes the anisotropy in the contact normal density and is loading sensitive. G_{ij}^v defines the anisotropy in the mean contact vector and has a close correlation with the particle orientation anisotropy. We can conveniently define a single fabric anisotropy tensor C_{ij} to reflect the combined influence of anisotropies of both contact normal density and mean contact vector as follows:

$$C_{ij} = G_{ij}^v + \frac{1}{2}D_{ij}^c. \tag{24}$$

Since G_{ij}^v and D_{ij}^c are deviatoric and symmetric tensors, the combined fabric anisotropy tensor C_{ij} is therefore also deviatoric and symmetric, expressed as

$$C_{ij} = G_{ij}^v + \frac{1}{2}D_{ij}^c = \Delta\begin{pmatrix} \cos\psi & \sin\psi \\ \sin\psi & -\cos\psi \end{pmatrix}, \tag{25}$$

where $\Delta = \sqrt{\left(B_1^v\right)^2 + \left(d_2^c\right)^2/4 + B_1^v d_2^c \cos\left(\beta_1^v - \phi_2^c\right)}$ gives information on the magnitude of the combined fabric anisotropy and $\psi/2$ indicates the principal fabric direction with $\tan\psi = \left[B_1^v \sin\beta_1^v + \left(d_2^c \sin\phi_2^c\right)/2\right] / \left[B_1^v \cos\beta_1^v + \left(d_2^c \cos\phi_2^c\right)/2\right]$.

With the single fabric anisotropy tensor defined by Eq. (24), the normalized deviatoric stress tensor becomes

$$\eta_{ij} = \frac{1}{1+h}\left(G^f_{ji} + C^v_{ij}\right). \tag{26}$$

For an isotropic specimen, the fabric anisotropy tensor $C^v_{ij} = 0$. The principal stress direction is always coaxial with the force anisotropy direction, and the stress ratio is the same irrespective of the loading direction. However, when the material fabric is anisotropic, the non-coincidence between the principal fabric direction and force direction leads to a variation in material stress ratio and a possible deviation between the principal stress direction and the force anisotropy direction.

3.2 Fabric anisotropy and stress ratio

With Eqs. (11), (24) and (26), the stress ratio can be found as:

$$\eta = \frac{2}{1+h}\left(\Delta + B^f_1\right)\left[1 - 2\frac{\Delta/B^f_1}{\left(\Delta/B^f_1 + 1\right)^2}\left(1 - \cos\left(\psi - \beta^f_1\right)\right)\right]^{1/2}. \tag{27}$$

This equation shows that stress ratio mobilized in a granular materials under shearing is determined by the magnitudes of fabric and force anisotropies, Δ and B^f_1. It is also affected by the non-coincidence between the principal directions of force and fabric anisotropies $\left(\psi - \beta^f_1\right)/2$. When fabric anisotropy and force anisotropy are coaxial, i.e. $\left(\psi - \beta^f_1\right)/2 = 0°$, the stress ratio is maximal and is equal to $\eta_0 = 2\left(\Delta + B^f_1\right)/(1+h)$. When there is a non-coincidence between the two principal directions $\left(\psi - \beta^f_1\right)/2$, the stress ratio becomes $\eta = \kappa\eta_0$, where

$$\kappa = \left[1 - 2\frac{\Delta/B^f_1}{\left(\Delta/B^f_1 + 1\right)^2}\left(1 - \cos\left(\psi - \beta^f_1\right)\right)\right]^{1/2}. \tag{28}$$

The value of κ is calculated from the ratio Δ/B^f_1 and the deviation in the two principal directions $\left(\psi - \beta^f_1\right)/2$. In Fig. 4, κ is plotted against $\left(\psi - \beta^f_1\right)/2$ at different values of Δ/B^f_1. It is shown that κ decreases with increasing $\left(\psi - \beta^f_1\right)/2$, indicating a smaller stress ratio when the fabric direction rotates away from the force direction towards being normal to it. The decrease in stress ratio becomes more significant when the ratio Δ/B^f_1 increases, suggesting that a larger fabric anisotropy causes a higher strength anisotropy. The stress ratio becomes zero, when $\Delta/B^f_1 = 1$ and $\left(\psi - \beta^f_1\right)/2 = 90°$.

3.3 Fabric anisotropy and principal stress direction

Using Eqs. (11), (24) and (26), we can also determine the principal stress direction $\theta_\sigma/2$. Denote $\theta/2 = \left(\theta_\sigma - \beta^f_1\right)/2$ as the angle between the principal stress direction and the principal direction of force anisotropy. We have $\theta_\sigma = \theta + \beta^f_1$, where the angle θ can be determined from

$$\tan\theta = \frac{\left(\Delta/B^f_1\right)\sin\left(\psi - \beta^f_1\right)}{\left(\Delta/B^f_1\right)\cos\left(\psi - \beta^f_1\right) + 1} \tag{29}$$

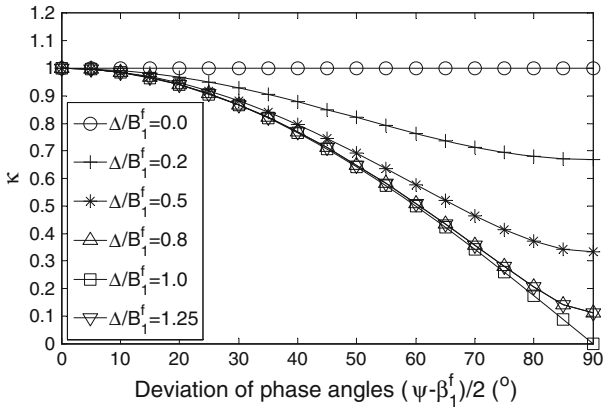

Fig. 4 The normalized stress ratio

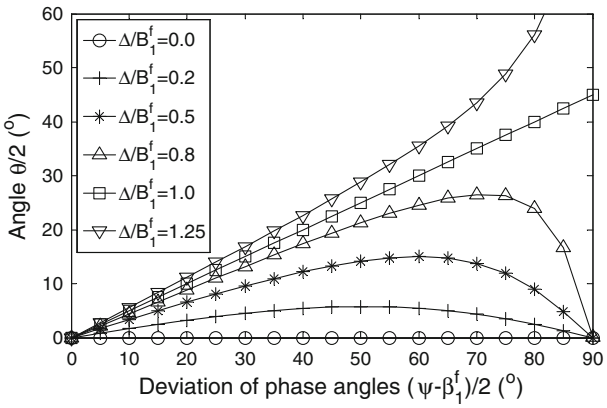

Fig. 5 The principal stress direction (after Li and Yu [25])

Figure 5 plots the principal stress direction in terms of $\theta/2$ at different values of Δ/B_1^f and $\left(\psi-\beta_1^f\right)/2$. When the fabric anisotropy is much smaller than the force anisotropy, i.e. the ratio Δ/B_1^f is small, the angle between the principal stress direction and the principal force direction is small with the maximum occurring around $\left(\psi-\beta_1^f\right)/2=45°$. When the fabric anisotropy is larger and becomes comparable with force anisotropy, the angle between the principal stress direction and the principal force direction increases and the maximal value skews towards higher $\left(\psi-\beta_1^f\right)/2$ values. With $\Delta/B_1^f=1$, the principal stress is always in the middle between the principal force direction and the principal fabric direction, i.e. $\theta=\left(\psi+\beta_1^f\right)/2$. When the ratio increases further so that $\Delta/B_1^f>1$, the principal stress direction becomes closer to the fabric anisotropy direction than the force anisotropy direction.

4 Numerical simulation results

In a study on material anisotropy, Li and Yu [22] prepared and tested two anisotropic specimens using discrete element modelling. Particles used in the simulations were formed by clumping two equal-sized discs together. The distance between the centres of the two discs was equal to 1.5 times the disc radius, r. The particle size was uniformly distributed within (0.2, 0.6) mm in terms of equivalent diameter, and the disc thickness was $t=0.2$ mm. The contact law included two constant stiffness models (normal and tangential) and a slip model. In the simulations, the elastic models were linear, and the particle stiffness was set to be $k_n=k_s=10^5$ N/m. The coefficient of friction was 0.5.

Each specimen was sheared in varying loading direction from vertical to horizontal with 15° intervals. One was the initially anisotropic sample prepared using the deposition method. The void ratio of the prepared sample was 0.204 at $p_c = 1{,}000$ kPa. The other was the preloaded sample, prepared by shearing the initially anisotropic sample vertically up to 25 % deviatoric strain and then unloading to isotropic stress state. The void ratio of the preloaded sample was 0.222 with the mean normal stress $p_c = 1{,}000$ kPa. The loading direction was denoted by the angle α, the deviation to the horizontal direction, i.e., x_1 axis direction. Loading is applied in a strain-controlled mode with the principal strain direction fixed. Shearing was carried out at constant confining stresses.

Further details of the numerical simulation are available in the paper [22]. Statistical analyses were carried out on the particle and contact information. Together with the insights provided by the theoretical SFF relationship, some of these numerical results are used here to facilitate our discussions on strength anisotropy and deformation non-coaxiality.

4.1 Fabric and force anisotropy

In Eq. (19), the contributions from the joint products of direction tensors have been taken into account in terms of the coefficient h, which affects the mean normal stress defined in Eq. (21) as well as the stress ratio defined in Eq. (27). For the two series of numerical simulations reported in [22], the coefficient h was found to increase as a result of the developments in fabric and force anisotropies and when their principal directions become more coaxial as shear continues. However throughout the whole shearing process, its magnitude remains small and its influence is considered secondary. Hence, in the following, we will mainly focus our discussion on the fabric anisotropy tensor C_{ij} and the force anisotropy tensor G^f_{ji} and consider the micromechanics of anisotropic granular materials in terms of their evolutions.

The evolution of fabric anisotropy and contact force anisotropy for the two series of tests are plotted in Figs. 6 and 7 in terms of the anisotropy magnitudes, Δ and B^f_1, and the phase angles, $\psi/2$ and $\beta^f_1/2$, respectively.

The two specimens have initially anisotropic structures, evidenced by the nonzero values of fabric anisotropy magnitudes. The principal fabric directions at the initial state were both vertical with $\psi/2 = 90°$. Before shearing, the stress state is isotropy with $\eta = 0$. At this state, $G^f_{ji} = -C^v_{ij}$ from Eq. (26). That is to say, the force anisotropy and the fabric anisotropy were of equal magnitudes, while their principal directions were normal to each other, as supported by the data points in the figures.

The fabric anisotropy for the preloaded specimen was larger than that of the initially anisotropic specimen at the initial state due to preloading. However in comparison with the preloaded specimen, the initially anisotropic specimen quickly developed higher fabric anisotropy in the loading direction. As for contact force anisotropy, the initially anisotropic specimen developed a high anisotropy magnitude at very low strain level, while the increase in the preload specimen was less rapid. This is possibly due to the difference in their void ratios.

Once shearing started, the principal direction of force anisotropy adjusted almost instantaneously to the imposed loading direction, while the principal direction of fabric anisotropy adjusted much slower. For all the simulations, the principal directions of force anisotropy were observed to be very close to the loading direction. The magnitudes of force anisotropy differed slightly when the loading direction changed, as seen in Fig. 7. As for fabric anisotropy, when its principal direction was non-coaxial with the loading direction, the principal fabric direction rotated and gradually approached the loading direction. During this process, the evolutions of the magnitudes of fabric anisotropy were observed to be different. When the loading was coaxial with the fabric anisotropy, the fabric anisotropy kept increasing upon shearing. The magnitudes of fabric anisotropy became smaller when the loading direction deviated further away from the principal fabric direction, and even experienced a temporary decrease in the case of $\alpha = 0°$, as seen in Fig. 6.

At large strain levels, the specimens approached critical states. Due to the differences in the relative direction between initial fabric and loading, material fabric goes through various paths to reach the ultimate state at which both the fabric anisotropy and the force anisotropy approached their respective critical magnitudes. Despite the differences in the loading directions and hence the early evolutions, the two anisotropic specimens approached the same critical state characterized by macroscopically the critical stress ratio $\eta_c = 0.85$, and microscopically, the critical material fabric anisotropy $\Delta_c = 0.18$ and the critical force anisotropy $\left(B^f_1\right)_c = 0.27$. At the critical state, the directions of both fabric anisotropy and force anisotropy were coaxial with the loading direction.

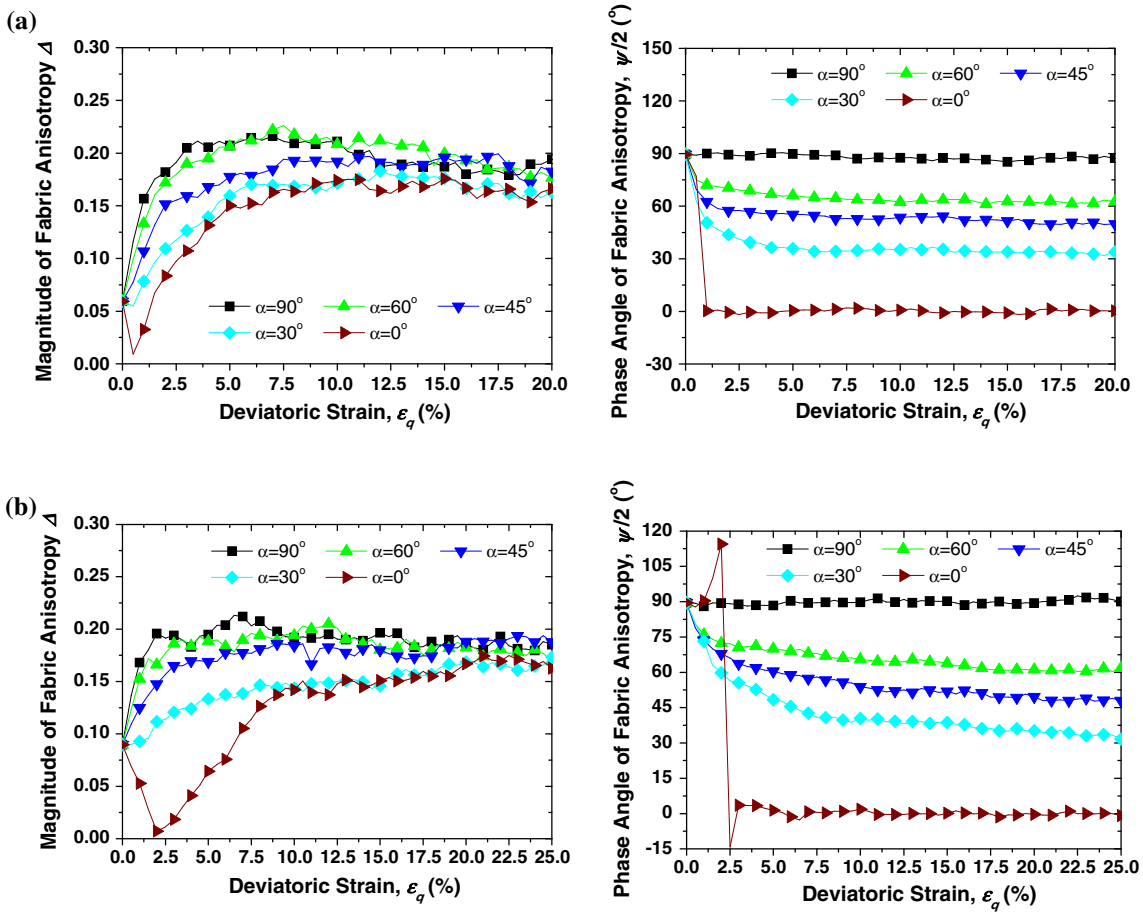

Fig. 6 Fabric anisotropy. **a** Initially anisotropic specimen. **b** Preloaded specimen

Material behaviour became coaxial, and the stress ratios for different loading directions became equal at the critical state.

4.2 Strength anisotropy

It should be noted that the stress ratio $\eta = q/p$, when reaching a peak value during shearing, can be converted into a peak angle of internal friction and is generally used to define shear strength of a granular materials [47]. Equation (27) provides an analytical expression of the mobilized stress ratio and can be used to study the micromechanics of material shear strength. For completeness, the evolutions of the mobilized stress ratio for the two series of simulations are shown in Fig. 8. The solid symbols are the stress measured on the specimen boundaries, while the hollow symbols are the predictions from Eq. (27). It is evident that the two sets of data are in good agreement and hence validate the use of Eq. (27). The specimens developed a larger stress ratio when the loading direction was closer to the principal fabric direction.

The stress ratio is given in terms of microparameters as defined in Eq. (27). Apart from the secondary parameter h, the stress ratio is mainly a function of the sum of the two magnitudes $\left(\Delta + B_1^f\right)$, the ratio of the two magnitudes Δ/B_1^f and the angle between the principal directions $\left(\psi - \beta_1^f\right)/2$. Figure 9 plots the evolutions of $\left(\Delta + B_1^f\right)$ for the two series of tests. Since the value of h is small, the plot of $\left(\Delta + B_1^f\right)$ is very informative in showing the variation of the maximal stress ratio as if the two anisotropies are coaxial. $\left(\Delta + B_1^f\right)$ seems to be the dominant influential parameter governing the stress ratio, supported by the close similarity between Figs. 8 and 9.

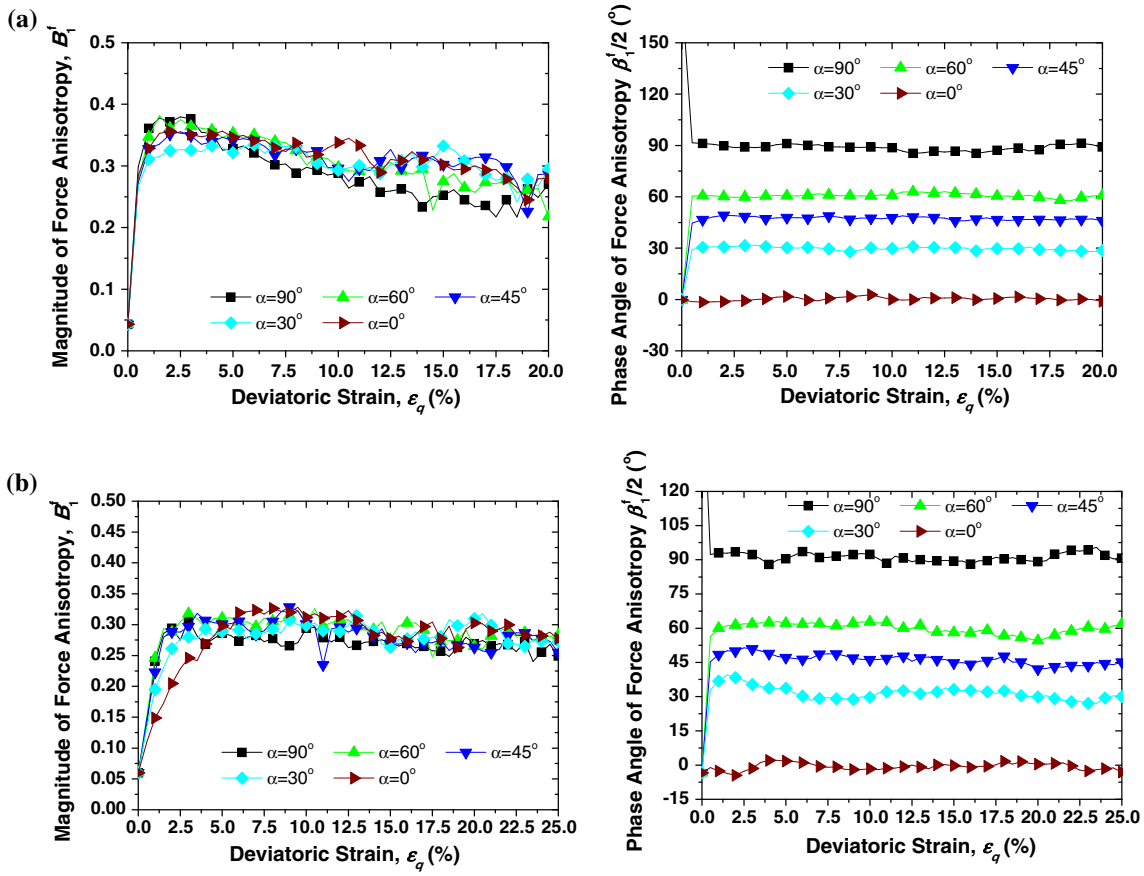

Fig. 7 Contact force anisotropy. **a** Initially anisotropic specimen. **b** Preloaded specimen

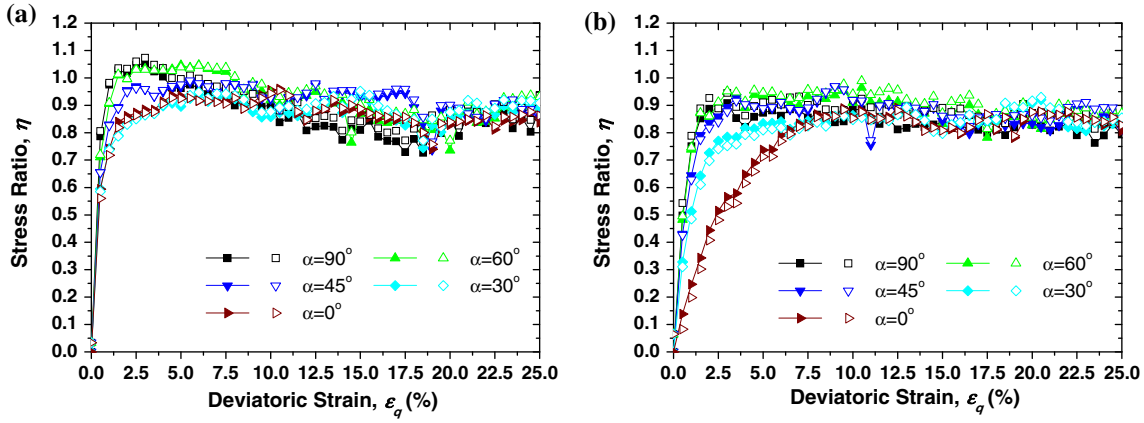

Fig. 8 Observations on strength anisotropy (after Li and Yu [25]) **a** Initially anisotropic specimen, **b** Preloaded specimen

The stress ratio is affected by the ratio of fabric anisotropy to force anisotropy Δ/B_1^f as a result of the non-coincidence between their principal directions. The non-coincidence between fabric anisotropy and force anisotropy can potentially further reduce material stress ratio by a factor of κ as evidenced in Eq. (29). Figure 4 plots κ in terms of the anisotropy ratio Δ/B_1^f and the angle $\left(\psi - \beta_1^f\right)/2$. In general, the magnitude of fabric anisotropy is smaller than that of force anisotropy ($\Delta/B_1^f < 1$). In this case, the larger the angle $\left(\psi - \beta_1^f\right)/2$, the larger the ratio Δ/B_1^f, the smaller the mobilized stress ratio becomes.

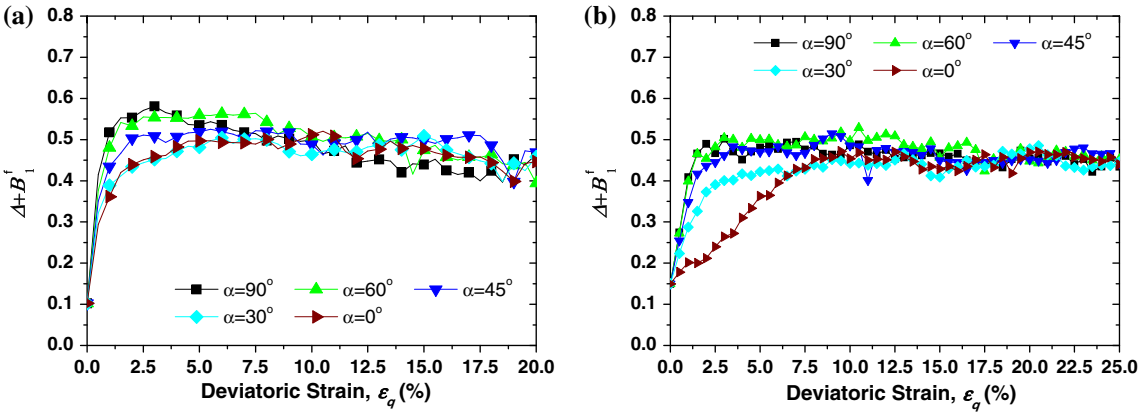

Fig. 9 Observations on $\left(\Delta + B_1^f\right)$ **a** Initially anisotropic specimen, **b** Preloaded specimen

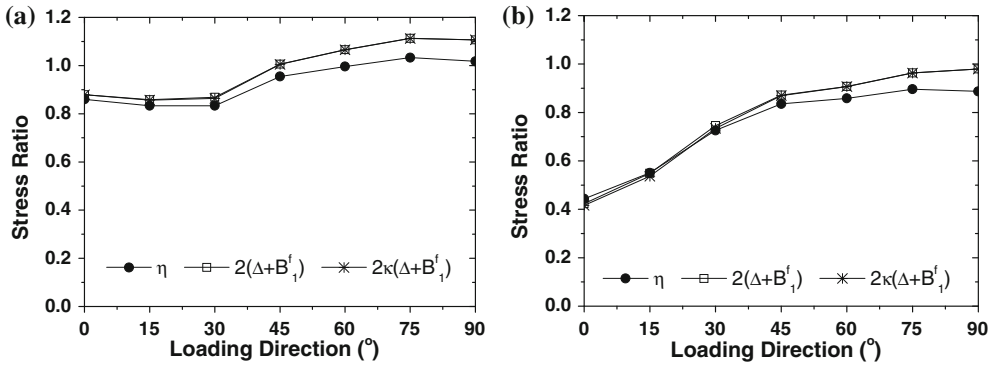

Fig. 10 Stress ratios at 2 % deviatoric strain level. **a** Initially anisotropic specimen, **b** Preloaded specimen

Figure 10 plots information of the stress ratio η together with $2\left(\Delta + B_1^f\right)$ and $2\kappa\left(\Delta + B_1^f\right)$ at 2 % of deviatoric strains, a strain level close to the occurrence of the peak stress ratio (i.e. material strength) in the dense samples. For comparison, information of both the initially anisotropy specimen and the preloaded specimen is presented. The figure gives clear evidence of strength characteristics of anisotropic granular materials. The observation was shown to be in qualitative agreement with the strength anisotropy of Portway sand [5] using a hollow cylinder apparatus. Slight differences between data points of $2\kappa\left(\Delta + B_1^f\right)$ and η were observed as a result of neglecting the joint product term h.

$2\left(\Delta + B_1^f\right)$ and $2\kappa\left(\Delta + B_1^f\right)$ are shown almost coincident with each other, suggesting that κ is close to 1 at 2 % of strain level. This can be explained based on the evolution of the ratio Δ/B_1^f and the angle $\left(\psi - \beta_1^f\right)/2$. When the loading direction is further away from the initial principal fabric direction, the angle between the two anisotropies $\left(\psi - \beta_1^f\right)/2$ is larger, while the ratio of Δ/B_1^f gets smaller. Even though force anisotropy and fabric anisotropy are still non-coaxial, the angle $\left(\psi - \beta_1^f\right)/2$ has reduced to less than 20° at 2 % of strain level. And the influence of non-coincidence between force and fabric is not notable.

Peak stress ratio develops at a strain level around 2 % or even larger, when the angle $\left(\psi - \beta_1^f\right)/2$ gets even smaller. Hence, at the strain level of material peak strength, κ is very close to 1. This suggests that material strength anisotropy is mainly consequential to the differences in the sum of the magnitudes of fabric anisotropy and force anisotropy $\left(\Delta + B_1^f\right)$.

Information of the fabric anisotropy degree Δ and the force anisotropy degree B_1^f is presented in Figs. 6 and 7. When the specimen was loaded in different directions, the degrees of force anisotropy differed but in a limited range, as seen in Fig. 7, while for fabric anisotropy, the evolutions of the magnitudes of fabric

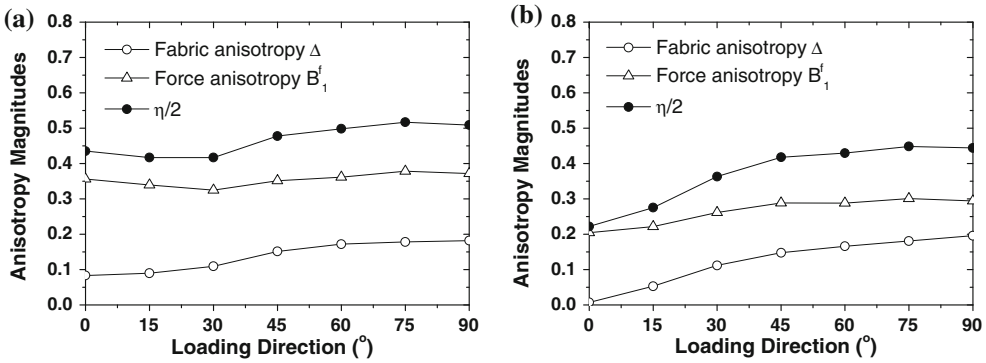

Fig. 11 Anisotropic magnitudes at 2 % of deviatoric strain level. **a** Initially anisotropic specimen, **b** Preloaded specimen

anisotropy were observed to be very sensitive to the loading direction. A large and monotonic increase was observed for the case $\alpha = 90°$ when the loading was coaxial with the fabric anisotropy. The magnitudes of fabric anisotropy became smaller, when the loading direction deviated further away from the principal fabric direction, and even experienced a temporary decrease in the case $\alpha = 0°$, as seen in Fig. 6. In a word, the variation of fabric anisotropy due to varying loading direction is more significant than that of force anisotropy.

Figure 11 compares the magnitudes of fabric anisotropy Δ and force anisotropy B_1^f at 2 % of deviatoric strain, for both the initially anisotropy specimen and the preloaded specimen. $\eta/2$ is also plotted in the same figure, bearing in mind that $\left(\Delta + B_1^f\right)$ is the governing parameter on $\eta/2$. It is observed that the magnitude of force anisotropy is in general larger than that of fabric anisotropy. This explains why the peak stress ratio is observed at around the same level of peak force anisotropy. Combining information in Figs. 6 and 7, we can see that after the peak, the continuous increase in the fabric anisotropy compensates partially the sharp drop in force anisotropy. The stress ratio hence softens gradually towards the critical stress ratio.

4.3 Deformation non-coaxiality

Supported by the observations in Fig. 7, we can assume that in monotonic shearing, the direction of force anisotropy is coaxial with the strain increment (i.e. loading direction). As a result, the degree of non-coaxiality is equal to the deviation of the principal stress direction from that of force anisotropy, i.e. $\theta/2$. As can be seen from Eq. (29), the degree of non-coaxiality is determined by the ratio Δ/B_1^f and the angle between contact force and material fabric $\left(\psi - \beta_1^f\right)/2$. The dependence of the degree of non-coaxiality on Δ/B_1^f and $\left(\psi - \beta_1^f\right)/2$ is shown in Fig. 5. The evolution of Δ/B_1^f and $\left(\psi - \beta_1^f\right)/2$ can be inferred by comparing the fabric and force anisotropies presented in Figs. 6 and 7. When the loading direction varies from horizontal ($\alpha = 0°$) to vertical ($\alpha = 90°$), the ratio Δ/B_1^f becomes larger, while the deviation in phase angle $\left(\psi - \beta_1^f\right)/2$ gets smaller.

For the initially anisotropic specimen, the contact force anisotropy increases rapidly upon shearing, and therefore, the ratio Δ/B_1^f is even smaller in comparison with that of the preloaded specimen. Referring to Fig. 5, when the ratio Δ/B_1^f is small, the degree of non-coaxiality is expected to small and the maximal degree of non-coaxiality appears at around $\alpha = 45°$. This explains our observations on the deformation non-coaxiality of the initially anisotropic specimen, as reproduced in Fig. 12a. In Fig. 12, the solid symbols are the data measured on the specimen boundaries, while the hollow symbols are the predictions from Eq. (29).

For the preloaded sample, the anisotropy in contact force increases less rapidly and the ratio Δ/B_1^f is higher than that of the initially anisotropic specimen, in particular in the small strain level. When the loading direction varies from horizontal ($\alpha = 0°$) to vertical ($\alpha = 90°$), the ratio Δ/B_1^f is observed to increase even further. At 2% of shear strain, the values of Δ/B_1^f in general lie within the range of (0.4, 0.6) except when $\alpha = 0°$ and $\alpha = 90°$. As can be seen from Fig. 5, we now expect a much more remarkable degree of non-coaxiality (up to 20°). Larger degrees of non-coaxiality appear when the loading direction is closer to the horizontal direction.

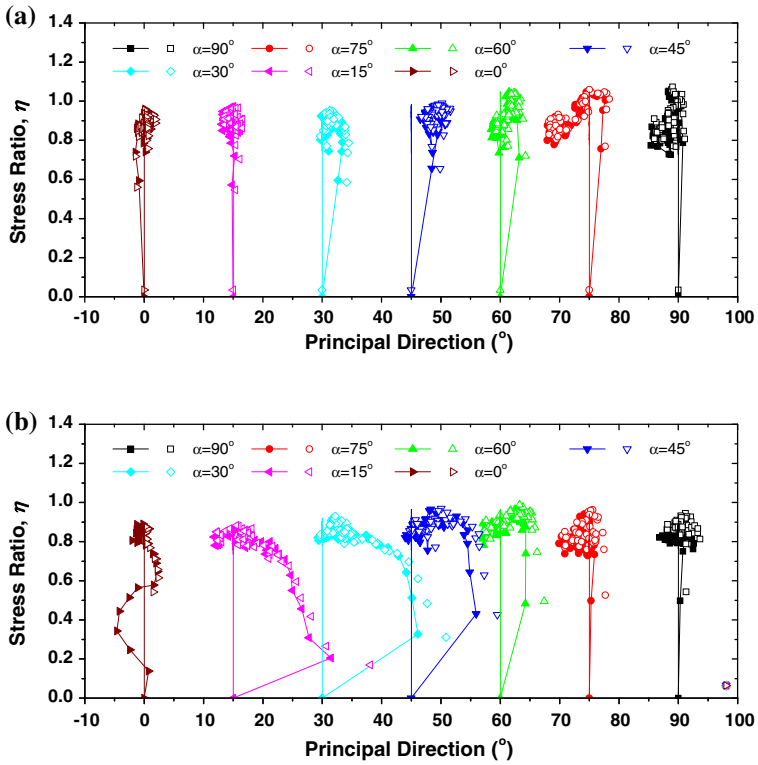

Fig. 12 Observations on deformation non-coaxiality (after Li and Yu [25]). **a** Initially anisotropic specimen. **b** Preloaded specimen

This explains the observation on the deformation non-coaxiality for the preloaded specimen, as reproduced in Fig. 12b.

In a summary, despite that the initially anisotropic sample and the preloaded sample are of similar anisotropic degrees before shearing, the ratio Δ/B_1^f in the preloaded specimen is much higher than that in the initially anisotropic specimen. As a result, it was observed for the preloaded sample that non-coaxiality between the principal directions of stress and strain increment was significant, but for the initially anisotropic sample, it was negligible.

5 Conclusions

The SFF relationship has been established using the directional statistical theory. It gives an analytical expression of the material stress tensor in terms of fabric and force direction tensors. In two dimensions, the SFF can be written in a very concise form, as given in Eq. (19). Based on the newly derived SFF and the DEM simulation results obtained from [22], we have investigated the micromechanics of anisotropic granular materials by focusing on fabric, force and strength anisotropies and their evolutions during shearing. The key findings of this investigation are given below:

- A combined, single, fabric anisotropy tensor C_{ij} can be used to take into account the effect of both contact normal density anisotropy and contact vector anisotropy.
- For the materials used in the DEM simulations, the magnitude of force anisotropy is generally larger than that of fabric anisotropy. In monotonic loading, once shearing started, the principal direction of force anisotropy adjusts almost instantaneously to the imposed loading direction, while the fabric anisotropy only gradually approaches the loading direction.
- At large strain levels, the specimens approach critical states characterized macroscopically by the critical stress ratio $\eta_c = 0.85$, and microscopically by the critical degree of fabric anisotropy $\Delta_c = 0.18$ and the critical degree of force anisotropy $\left(B_1^f\right)_c = 0.27$. At the critical states, the directions of both fabric anisotropy and force anisotropy are coaxial with the loading direction.

- Material strength anisotropy has been shown to be mainly due to the differences in the sum of the degrees of fabric anisotropy and force anisotropy $\left(\Delta + B_1^f\right)$. Between these two, the variation of fabric anisotropy due to varying loading direction contributes more to strength anisotropy than that of force anisotropy. It is also potentially affected by the non-coincidence between the principal directions of force and fabric anisotropies $\left(\psi - \beta_1^f\right)/2$ depending on the ratio of these two magnitudes Δ / B_1^f as demonstrated in Fig. 4. However, its influence is believed negligible at the strain level of peak and critical stress ratio.
- Noting that in monotonic shearing, the direction of force anisotropy is coaxial with the loading direction, the degree of non-coaxiality can be estimated by Eq. (29). It depends on the ratio between the degrees of fabric and force anisotropies Δ / B_1^f and the deviation between their directions $\left(\psi - \beta_1^f\right)/2$. It is found that the degree of deformation non-coaxiality becomes significant only if: a) the ratio between the degree of fabric anisotropy and the degree of force anisotropy is sufficiently large, and b) the principal fabric direction is sufficiently different from the applied loading direction.

Acknowledgments The work reported in this paper is financially supported by The University of Nottingham, UK. The authors would like to thank the reviewers for their careful reading and constructive comments that have contributed to the quality of the manuscript.

References

1. Ai, J., Langston, P.A., Yu, H.-S.: Discrete element modelling of material non-coaxiality in simple shear flows. Int. J. Numer. Anal. Methods Geomech. doi:10.1002/nag.2230
2. Arthur, J.R.F., Chua, K.S., Dunstan, T.: Induced anisotropy in a sand. Geotechnique **27**(1), 13 (1977)
3. Arthur, J.R.F., Menzies, B.K.: Inherent anisotropy in a sand. Geotechnique **22**(1), 115–128 (1972)
4. Bagi, K.: Stress and strain in granular assemblies. Mech. Mater. **22**(3), 165–177 (1996)
5. Cai, Y., Yu, H.S., Wanatowski, D., Li, X.: Non-coaxial behaviour of sand under various stress paths. J. Geotech. Geoenviron. Eng. ASCE **37**(1), 75–96 (2013)
6. Casagrande, A., Carrillo, N.: Shear failure of anisotropic materials. Proc. Boston Soc. Civil Eng. **31**, 74–87 (1944)
7. Christoffersen, J., Mehrabadi, M.M., Nemat-Nasser, S.: A micromechanical description of granular material behaviour. J. Appl. Mech. ASME **48**, 339–344 (1981)
8. Cundall, P.A., Strack, O.D.L.: A discrete numerical model for granular assemblies. Geotechnique **29**(1), 47–65 (1979)
9. Dafalias, Y.F.: An anisotropic critical state soil plasticity model. Mech. Res. Commun. **13**(6), 341–347 (1986)
10. Drescher, A.: An experimental investigation of flow rules for granular materials using optically sensitive glass particles. Geotechnique **26**(4), 591–601 (1976)
11. Drescher, A., Josselinde Jong, G.De : Photoelastic verification of a mechanical model for the flow of a granular material. J. Mech. Phys. Solids **20**, 337–351 (1972)
12. Goddard, J.: An elastohydrodynamics theory for the rheology of concentrated suspensions of deformable particles. J. Non-Newton. Fluid Mech. **2**, 169–189 (1977)
13. Gutierrez, M., Ishihara, K., Towhata, I.: Flow theory for sand rotation of principal stress direction. Soils Found. **31**, 121–132 (1991)
14. Hall, S.A., Bornert, M., Desrues, J., Pannier, Y., Lenoir, N., Viggiani, G., Besuelle, P.: Discrete and continuum analysis of localised deformation in sand using X-ray micro CT and volumetric digital image correlation. Geotechnique **60**(5), 315–322 (2010)
15. Itasca Consulting Group Inc.: PFC2D (Particle Flow Code in Two Dimensions), version 3.1ICG, Minneapolis (1999)
16. Kanatani, K.-I.: Distribution of directional data and fabric tensors. Int. J. Eng. Sci. **22**(2), 149–164 (1984a)
17. Kanatani, K.: Distribution of directional data and fabric tensors. Int. J. Eng. Sci. **22**(2), 149–164 (1984b)
18. Konishi, Y., Oda, M., Nemat-Nasser, S.: Deformation and failure of granular materials. In: Proc., Proc. IUTAM Conf. Balkema, Rotterdam, pp. 403–412 (1982)
19. Lade, P.V.: Failure criterion for cross-anisotropic soils. J. Geotech. Geoenviron. Eng. **134**(1), 117–124 (2008)
20. Lade, P.V., Duncan, J.M.: Elastoplastic stress-strain theory for cohesionless soil. J. Geotech. Eng. ASCE **101**, 1037–1053 (1975)
21. Lam, W.-K., Tatsuoka, F.: Effects of initial anisotropic fabric and $\sigma 2$ on strength and deformation characteristics of sand. Soils Found. **28**(1), 89–106 (1988)
22. Li, X., Yu, H.-S.: Influence of loading direction on the behaviour of anisotropic granular materials. Int. J. Eng. Sci. **47**, 1284–1296 (2009)
23. Li, X., Yu, H.-S.: Tensorial Characterisation of Directional Data in Micromechanics. Int. J. Solids Struct. **48**(14-15), 2167–2176 (2011)
24. Li, X., Yu, H.-S.: On the stress–force–fabric relationship for granular materials. Int. J. Solids Struct. **50**(9), 1285–1302 (2013)
25. Li, X., Yu, H.-S.: Particle scale insight into deformation non-coaxiality of granular materials. Int. J. Geomech. doi:10.1061/(ASCE)GM.1943-5622.0000338

26. Li, X., Yu, H.-S., Li, X.-S.: Macro-micro relations in granular mechanics. Int. J. Solids Struct. **46**(25-26), 4331–4341 (2009)
27. Li, X.S., Dafalias, Y.F.: A constitutive framework for anisotropic sand including non-proportional loading. Geotechnique **54**(1), 41–55 (2004)
28. Love, A.E.H.: A Treatise of Mathematical Theory of Elasticity. Cambridge University Press, Cambridge (1927)
29. Miura, K., Miura, S., Toki, S.: Deformation behavior of anisotropic dense sand under principal stress axes rotation. Soils Found. **26**(1), 36–52 (1986)
30. Nakata, Y., Hyoda, M., Murata, H., Yasufuku, N.: Flow deformation of sands subjected to principal stress rotation. Soils Found. **38**(2), 115–128 (1998)
31. Ng, T.T.: Numerical simulations of granular soil using elliptical particles. Comput. Geotechn. **16**, 153–169 (1994)
32. Oda, M., Koishikawa, I., Higuchi, T.: Experimental study of anisotropic shear strength of sand by plane strain test. Soils Found. **18**(1), 25–38 (1978)
33. Oda, M., Nakayama, H.: Yield function for soil with anisotropic fabric. J. Eng. Mech. **115**(1), 89–104 (1989)
34. Oda, M., Nemat-Nasser, S., Konishi, J.: Stress-induced anisotropy in granular masses. Soils Found. **25**(3), 85–97 (1985)
35. Ouadfel, H., Rothenburg, L.: Stress-force-fabric' relationship for assemblies of ellipsoids. Mech. Mater. **33**, 201–221 (2001)
36. Roscoe, K.H., Basssett, R.H., Cole, E.R.: Principal axes observed during simple shear of a sand. In: Proceedings of the Geotechnical Conference, vol. 1, pp. 231–237. Oslo (1967)
37. Rothenburg, L., Bathurst, R.J.: Analytical study of induced anisotropy in idealised granular material. Geotechnique **39**(4), 601–614 (1989)
38. Rothenburg, L., Bathurst, R.J.: Influence of particle eccentricity on micromechanical behavior of granular materials. Mech. Mater. **16**(1-2), 141–152 (1993)
39. Rothenburg, L., Selvadurai, A.P.S. : A micromechanical definition of the Cauchy stress tensor for particulate media. In: Selvadurai, A.P.S (ed.) Proceedings of the International Symposium on Mechanical Behaviour of Structured Media, pp. 469–486. Canada, Ottawa (1981)
40. Satake, M: Fabric tensor in granular materials. In: Luger, V.A. (ed.) Deformation and Failure of Granular materials, pp. 63–68. Balkema, Amsterdam (1982)
41. Thornton, C.: Numerical simulations of deviatoric shear deformation of granular media. Geotechnique **50**(1), 43–53 (2000)
42. Wan, R.G., Guo, P.J.: Stress dilatancy and fabric dependencies on sand behaviour. J. Eng. Mech. **130**(6), 635–645 (2004)
43. Weber, J.D.: Recherches concernant les contraintes intergranulaires dans les milieux pulvérulents. Bulletin de Liaison Laboratoire Des Ponts Et Chaussées **20**(3), 1–20 (1966)
44. Wong, R.K.S., Arthur, J.R.F.: Sand sheared by stresses with cyclic variations in direction. Geotechnique **36**(2), 215–226 (1986)
45. Yang, L.T.: Experimental study of soil anisotropy using Hollow Cylinder testing. Ph.D, University of Nottingham, Nottingham (2013)
46. Yoshimine, M., Ishihara, K., Vargas, W.: Effects of principal stress direction and intermediate principal stress on undrained shear behaviour of sand. Soils Found. **38**(3), 179–188 (1998)
47. Yu, H.S.: Plasticity and Geotechnics. Springer, Berlin (2006)